

## Electrically tuneable terahertz metasurface enabled by a graphene/gold bilayer structure

Andrew D. Squires<sup>1</sup> <sup>✉</sup>, Xiang Gao<sup>1,2</sup>, Jia Du<sup>1</sup>, Zhaojun Han<sup>1</sup>, Dong Han Seo<sup>1,3</sup>, James S. Cooper<sup>1</sup>, Adrian T. Murdock<sup>1</sup>, Simon K. H. Lam<sup>1</sup>, Ting Zhang<sup>1,4</sup> & Tim van der Laan<sup>1</sup> <sup>✉</sup>

Reconfigurable terahertz electronics devices with high tuneability are pivotal for next-generation high speed wireless communication and sensing technologies. Significant challenges exist for realizing these devices, particularly on the design of smart metastructures that can manipulate electromagnetic radiation at the terahertz frequencies and the fabrication of devices with effective tuneability and reconfigurability. Here, we incorporate graphene into a graphene/gold bilayer superimposed metamaterial structure, which enables efficient electrical tuning of terahertz waves. A 0.2 THz frequency-selective absorber is designed and experimentally developed using this graphene/gold bilayer metamaterial approach. The device demonstrates 16 dB amplitude tuning at 0.2 THz resonance and over 95% broadband modulation at just 6 V bias voltage while maintaining a benchmark high-quality factor resonance performance. The design and fabrication methods presented can be readily applied to produce a myriad of tuneable terahertz devices required for high-speed, reconfigurable THz wireless communication and sensing technologies.

<sup>1</sup>CSIRO Manufacturing, 36 Bradfield Road, Lindfield, NSW 2070, Australia. <sup>2</sup>School of Information and Electronics, Beijing Institute of Technology, Haidian District, Beijing 100081, China. <sup>3</sup>Energy Materials & Devices, Korea Institute of Energy Technology (KENTECH), Naju, Republic of Korea. <sup>4</sup>Global Big Data Technology Centre, University of Technology Sydney (UTS), P. O. Box 12315 Broadway, Sydney, NSW 2007, Australia. ✉email: [Andrew.squires@csiro.au](mailto:Andrew.squires@csiro.au); [Tim.vanderlaan@csiro.au](mailto:Tim.vanderlaan@csiro.au)

Rapidly increasing demands for high data-rate wireless communications and super-resolution imaging have pushed carrier frequencies of wireless systems towards higher spectral regions, millimeter wave (mmW) and terahertz (THz) bands<sup>1</sup>. In the THz region (0.1–3 THz), ultra-high bandwidths facilitate high-speed communications at data rates up to terabits per second<sup>2</sup>, making it ideal for next-generation wireless networks, e.g., 6G telecommunications. The development of THz wireless communication technologies, however, has been hampered by a lack of materials and devices that can perform beyond the limits of current electronic and photonic frequencies. Therefore, new materials, such as two-dimensional (2D) materials like graphene, and device configurations that feature ultrafast charge carrier dynamics and required functionalities (e.g., reconfigurability and tuneability) are in high demand to realize electronic and photonic devices operating at THz frequencies.

Electronic systems at THz frequency bands are usually accompanied by relatively high spurious tones and parasitic intermodulation due to frequency multiplication, heterodyne mixing, and amplification networks<sup>3</sup>. Frequency-selective absorbers<sup>4</sup> are required for eliminating undesirable interferences. Practical devices require electrical tuning of absorption amplitudes, and/or frequency, as parasitic interferences are usually highly sensitive<sup>5</sup>. These absorptions/resonances are characterized by their quality factor (Q-factor), defined as the resonant frequency divided by its full width at half maximum (FWHM). Electrically tuneable, frequency-selective THz absorbers with high Q-factor resonances are in high demand for designing THz systems, yet remain elusive<sup>5</sup>.

Metamaterials or metasurfaces consist of periodic arrays of subwavelength unit cells, which exhibit properties unattainable from natural materials by imitating the periodicity of the crystal lattice<sup>6</sup>. These structures allow the control and manipulation of the amplitude, polarization, and phase of electromagnetic waves, including THz waves<sup>7</sup>. However, a lack of tuneable devices in the THz region has led to a growing interest in 2D materials and metamaterials to enable tuneable, reconfigurable, and programmable properties for THz applications<sup>8</sup>. These metamaterial devices are essential for high-value, emerging applications, including target tracking, THz communications, THz sensing, and THz imaging<sup>7</sup>.

Graphene-based metamaterials have attracted significant attention for THz devices<sup>9</sup>. This attention is due to its unique electrical properties, including (i) high charge carrier mobility allowing ultrafast (THz) responses to electromagnetic fields; (ii) an electronic band structure featuring linear dispersion where charge transport is dominated by massless Dirac Fermions; and (iii) electric field-tuneable electrical conductivity. Proof-of-concept studies have confirmed the control of THz electromagnetic radiation with field-tuneable graphene films<sup>10</sup>. These have been adapted into fundamental components, such as modulators<sup>11–13</sup>, as well as stacked sandwich structures<sup>14</sup>. These studies instigated a plethora of theoretical studies investigating graphene-coupled THz metamaterial device designs, including (but not limited to) modulators<sup>15</sup>, absorbers<sup>16,17</sup>, filters<sup>18</sup>, switches<sup>19</sup>, sensors<sup>20</sup>, amplifiers<sup>21</sup>, and antennas<sup>22</sup>. However, the experimental realization of these theoretical devices is still in its infancy. This is due to difficulties in handling, fabrication, micro- and nano-patterning, and integration of graphene thin films into functional devices without significantly affecting the corresponding electrical properties. Further constraints are observed in producing reliable, uniform, and high-quality large-area graphene thin films.

Fabrication of graphene into practical, scalable, and functional electronic devices remains one of the most challenging parts of developing graphene-based electronics<sup>23</sup>. The limited experimental

graphene-based THz metamaterial devices reported to date use either an unpatterned graphene sheet hybridized with a patterned metal structure or simple graphene patches/geometries overlaid on sections of more complicated metal metastructures. Consequently, the reported graphene-based tuneable THz metamaterial devices often suffer low Q-factor resonances, poor tuneability, or have to operate at impractical high bias voltages. New metamaterial structures and fabrication methods are needed to advance the state-of-the-art graphene-based tunable metamaterial devices.

In this work, we present a graphene and gold bilayer metamaterial structure to address the lack of tunability of gold metasurfaces and the poor performance of graphene metasurfaces. A highly tuneable THz frequency-selective absorber is designed and experimentally developed to demonstrate the superiority of this bilayer approach. To the best of our knowledge, this is the first graphene metamaterial-based device reported operating in the 0.1–1 THz communications window, where graphene itself is patterned into the entire complex metasurface structure, producing a benchmark high-quality resonance (Q-factor up to 19) with large amplitude tuning (16 dB) at low bias (6 V). The design theory, simulation, and experimental results are presented; and the tuning mechanism is discussed. The device is built on a flexible, high-frequency laminate circuit board widely used in wireless communications components. The fabrication method is scalable and readily adapted to a wide range of THz devices that, currently, have only been theoretically modeled. This paves a way for developing the next generation of advanced metamaterial-based reconfigurable THz devices for wireless communication and sensing technologies.

## Results and discussion

**Metadevice design and modeling.** The schematic design of the THz metasurface absorber is detailed in Fig. 1a–c and a fabricated device image is shown in Fig. 1d. The device is a sandwich structure implemented on a 20 mm × 20 mm flexible, 0.254 mm thick glass-filled PTFE substrate (Rogers5880 Duroid). The top layer is comprised of a graphene thin film transferred onto a gold thin film (200 nm), deposited on the substrate, forming the graphene/gold bilayer. The bilayer is patterned and etched together so that the gold metasurface and graphene metasurface superimposes (highlighted by the dashed box in Fig. 1b). The bottom of the sandwich consists of a gold thin film (200 nm, on the back of the substrate) forming a radio-frequency (RF) ground. The metasurface design features a large array of Jerusalem-cross slots with unit cell dimensions of 450 μm × 450 μm. A Jerusalem-cross-slot structure is chosen to achieve a high Q-factor (high-frequency selectivity). This structure features long resonant paths for electric currents, which leads to smaller unit size and a more compact layout. The cross slots are also advantageous in minimizing the device sensitivity to the incident angle of the THz radiation. The image in Fig. 1d clearly shows a high-quality patterned graphene/gold bilayer device with well-defined features.

The metasurface absorber is modeled as an equivalent resistance, inductance, capacitance (RLC) resonant circuit, where the incident THz radiation is generated from an equivalent source circuit as shown in Fig. 2a. The equivalent inductance,  $L_A$ , and capacitance,  $C_A$ , is extracted from the metasurface structure with the resistance,  $R_A$ , extracted from the conductivity of the graphene/gold bilayer and dissipation properties of the Rogers5880 substrate. The source impedance,  $Z_S$ , corresponds to the wave impedance of the THz radiation. For an angular frequency,  $\omega$ , the input impedance of the equivalent load circuit is

$$Z_{\text{in}} = R_A + j\omega L_A - j \frac{1}{\omega C_A} \quad (1)$$

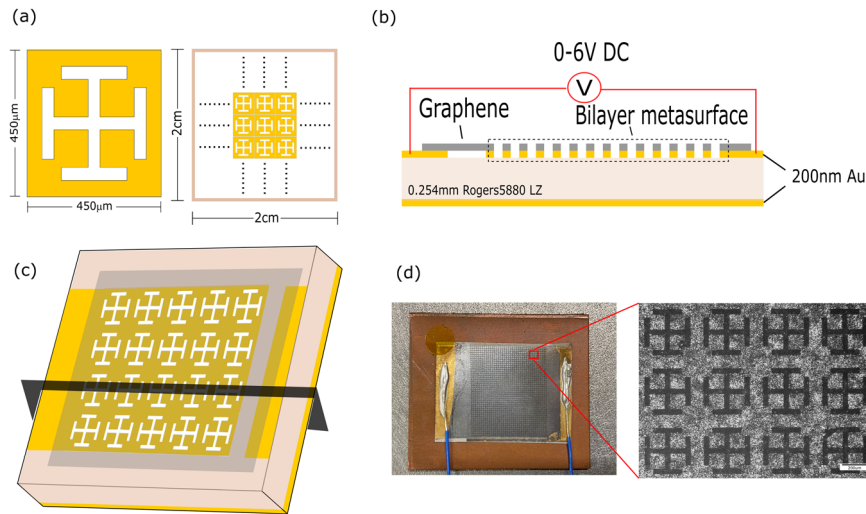


**Fig. 1** Summary of the graphene/gold bilayer metasurface incorporated into a 0.2 THz frequency-selective absorber. **a** Jerusalem-cross-slot unit cell dimensions and array structure. **b** Cross section of the graphene/gold bilayer superimposed metasurface structure indicated from the intersecting black plane in **(c)**. **c** Schematic of the 0.2 THz frequency-selective absorber device. **d** Fabricated bilayer device with an enlarged optical image showing well-defined metasurface structure.

The reflection coefficient,  $S_{11}$ , can be described as

$$S_{11} = 20 \log_{10} \left| \frac{Z_{in} - Z_S}{Z_{in} + Z_S} \right| \quad (2)$$

Here,  $S_{11}$  refers to the power ratio of electromagnetic radiation (THz) incident on the device to that reflected by the device. As such, the absorber is treated as a single-port device which can be directly compared to an experimental THz time-domain spectroscopy (TDS) measurement (see Methods). At the resonant frequency,  $Z_{in}$  has a real value and is equal to  $R_A$ . According to Eq. (2), the lowest reflection occurs where the resonant resistance  $R_A$  is well-matched with  $Z_S$ , which leads to a maximum power absorption of the metasurface absorber.

To investigate the electromagnetic behavior of the frequency-selective metasurface absorber and optimize its overall performance, detailed three-dimensional full-wave modeling and simulations are carried out by using the software CST Microwave Studio. Figure 2b–e shows the simulated electric field and current distributions within a unit cell of the bilayer metasurface absorber. As shown in Fig. 2b, c, the electric fields mainly concentrate near the horizontal slots and are much weaker elsewhere in the Jerusalem-cross-slot structure. This is because the incident THz radiation is vertically polarized, which can excite a strong electric field within the horizontal slot with a length similar to the resonant wavelength. Figure 2d, e show the vector and magnitude of the electric current distributions, respectively. Stronger electric currents concentrate near the two loaded slots at the end of the horizontal slot. This phenomenon can be readily understood by considering a position where the electric field achieves minimum, the electric current achieves maximum for the resonant mode.

When a THz wave propagates towards the absorber, it excites a resonant field mode within the 3D structure consisting of the metasurface and ground layer sandwiched by a Rogers substrate. At resonance, the THz power is well-absorbed due to the limited conductivity of the bilayer and dissipation properties of the Rogers5880 substrate. In this case, there is very little power reflected back towards the incident direction. Hence, the presented metasurface absorber exhibits good resonant absorption performance. The graphene/gold bilayer structure produces a strong resonance at 0.192 THz. The tuneable conductivity of the graphene in the bilayer implies the resistive component of the

circuit model is now adjustable, as shown in Eq. 3, which permits tuning of the output resonance.

$$R_A(V_A) = R_{\text{Gold}} + R_{\text{Graphene}} + \Delta R_{\text{Graphene}}(V_A) \quad (3)$$

Where  $\Delta R_{\text{Graphene}}$  corresponds to the change in graphene's resistance introduced by an applied voltage,  $V_A$ .

Figure 3 shows the simulation results, where the resonant amplitude can be theoretically tuned by 17 dB for a graphene conductivity range of 40–250 mS. Here, 40 mS corresponds to the unbiased case and was chosen from the experimental conductivity obtained for our unbiased graphene film through THz time-domain spectroscopy (see Supplementary Fig. 1). This result suggests that exceptionally efficient tuning can be obtained by implementing the graphene/gold bilayer approach.

**Fabrication of the metasurface device.** Prior to generating the graphene/gold bilayer concept, gold-only metasurface and graphene-only metasurface devices of the same design have been experimentally developed and characterized. A gold-only metasurface was simulated, fabricated, and measured to verify the device's theoretical design. Good agreement was found between experiment and simulation, as shown in Fig. 4 (red curves), thus validating the metadvice design theory. The measured experimental resonance, however, is slightly wider and stronger than in the simulation, which is likely due to minor fabrication imperfections and slightly higher conductive/substrate losses than those used in the model due to the natural variation of the products from the manufacturer's specifications. The full response over a wider 0.1–1 THz range, including other non-targeted resonances, is also supplied in Supplementary Fig. 2.

A simple approach to add tuneability to the gold-only metasurface device was to transfer an unpatterned graphene film over the top of the fabricated metasurface. This, however, led to the complete suppression of resonant behavior (see Supplementary Fig. 3). Graphene provides conduction pathways across the cross-slot gaps as well as partially blocking the THz waves transmitting into the array, likely causing this suppression. Another approach to introduce tuning to the device was to directly pattern the metasurface into graphene. A graphene-only metasurface device of the same design was fabricated and found to not possess observable resonant behavior up to 50 V applied

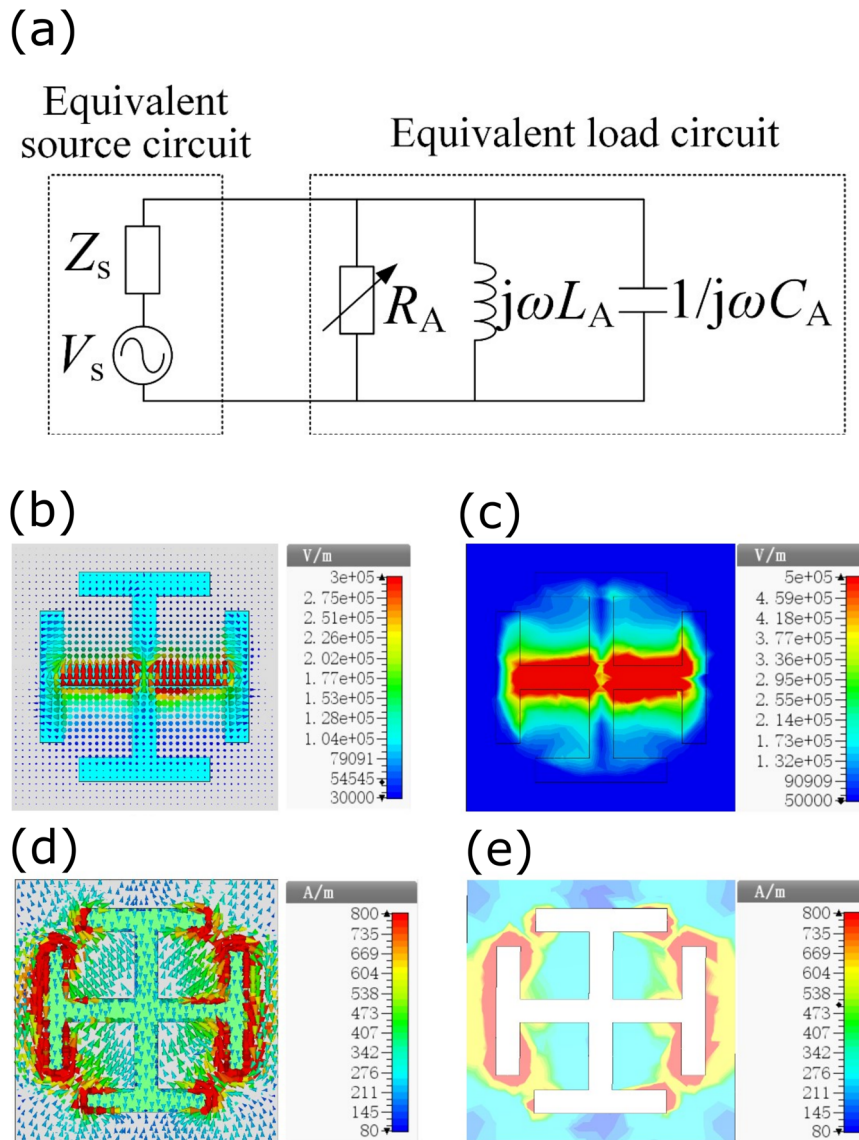


**Fig. 2 Modeling and simulation of the Jerusalem-cross-slot metasurface.** **a** Equivalent circuit model. **b** The vector of the electric field. **c** The magnitude of the electric field. **d** The vector of electric current. **e** The magnitude of electric current.

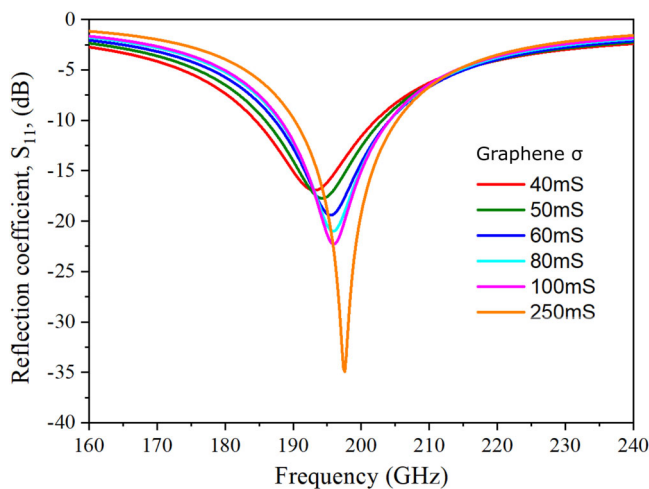


**Fig. 3 Simulation results of the bilayer metasurface at 0.2 THz.** Simulated  $S_{11}$  parameters for the graphene/gold bilayer metasurface device for a range of graphene conductivities from 40 to 250 mS.

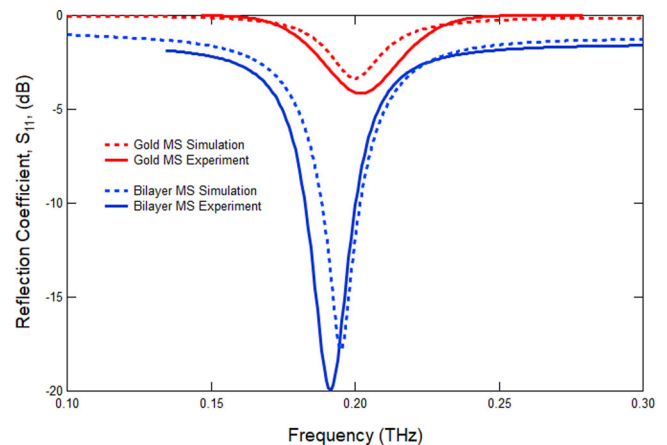


**Fig. 4 Comparison of experimental and simulated devices.** Experimentally measured  $S_{11}$  parameters (solid lines) of the unbiased gold-only (red) and graphene/gold bilayer (blue) metasurfaces compared to the simulation results (dashed lines).

voltage (see Supplementary Fig. 3). This was likely due to high losses in the graphene film, which damps away the resonance (i.e., very poor Q-factor). This result is consistent with those reported in literature where graphene significantly deteriorates the device performance (indicated by low Q-factors).

To solve the problems described above, a bilayer configuration was subsequently developed in this work. The bilayer approach takes advantage of the gold and graphene material properties collectively: a high-quality, low loss resonance from the patterned gold structure and a voltage-controlled tuneability from the graphene. In addition, the bilayer provides a simpler method for electrostatic tuning as the bilayer itself can be formed as one of the biasing electrodes.

To achieve the bilayer tuneable device, several challenges had to be addressed. This included developing (i) a suitable, large area, uniform graphene film, (ii) a graphene transfer method, which provides good adhesion to both gold and the dielectric substrate with minimal transfer residues, and (iii) a patterning method, which etches both the graphene and gold together in the bilayer. Any sample where the graphene was not sufficiently uniform (patchy flakes or containing microholes), or the transfer process introduced large wrinkles/delamination would result in a failed device.

The bilayer device was fabricated on a flexible commercial 0.254 mm thick Rogers 5880LZ laminate substrate. The RF ground was prepared with 220 nm of the sputtered gold film. The obverse side received the same gold deposition with a hard mask to define the metasurface area and contact regions. Chemical vapor deposition (CVD) graphene thin films on Nickel<sup>24</sup> (cut to 25 mm × 25 mm) were transferred onto the pre-prepared Rogers laminate using standard wet transfer techniques. More information about graphene synthesis and transfer is provided in the Methods section. The graphene/gold bilayer metasurface pattern was subsequently produced using a photolithography procedure, that is, spin-coating photoresist, ultraviolet light exposure, and photoresist development. The device chip with the photomask protection layer was etched using a reactive ion etching in alternative gases. Firstly, an O<sub>2</sub> plasma to remove the unprotected graphene, followed by etching in Ar (a chemically inert gas) to remove the unprotected gold layer, and finally, a short, final O<sub>2</sub> plasma etching was applied to clean the device. Electrical connection to external wires was made using silver epoxy on gold contacts in the device chip.

Through optimizing the graphene production, transfer, and device patterning (including etching), we have successfully established a process capable of reproducing well-defined micro-patterned graphene/gold bilayer metasurfaces as depicted in Fig. 1d. There is good agreement between simulation and experiment (Fig. 4 blue curves) for the bilayer metasurface, with a slightly higher resonant amplitude and bandwidth in the fabricated device. The strong agreement between simulation and measured responses for both the gold-only and graphene/gold metasurfaces suggests our model provides a valid prediction of the bilayer device performance. This also suggests a tuning functionality can be realized in gold-only THz metasurfaces by replacing the gold metasurface with a graphene/gold bilayer. Further device development, scanning electron microscopy (SEM) images and Raman mapping can be found in Supplementary Figs. 4–6.

**Tuneable performance at 0.2 THz.** THz time-domain spectroscopy (THz-TDS) is used to study the performance of the metasurface absorber (the measurement setup is shown and described in the Methods section). For the THz power spectrum, the scattering parameter,  $S_{11}$  is defined as  $S_{11} = 10\log(\text{Ref}(\omega))$ , where  $\text{Ref}(\omega)$  is the reflectance obtained directly from the THz-

TDS measurement. The  $S_{11}$  parameter allows the measured performance of the device to be compared to the modeled response.

Figure 5a shows the  $S_{11}$  parameter for the graphene/gold bilayer absorber at the designed 0.2 THz resonance with an applied voltage ranging from 0 to 6 V. Very efficient amplitude tuning is obtained when the voltage is changed. There is a 16 dB change of the signal at 0.2 THz for a low bias voltage of 6 V. This amplitude tuning is notably stronger than previously reported electrostatically tuned graphene THz metamaterials (below 3 dB)<sup>25–29</sup>.

The Q-factor, which is an important parameter for practical THz resonator absorbers, is 19 (at 6 V) for the measured bilayer resonance structure. This is significantly higher than other reported graphene THz metamaterial designs (all below 7)<sup>25–28,30–32</sup>. This is important as low Q-factors have limited the applicability of electrically tuneable THz devices based on graphene<sup>25</sup>. It is noted that the previous devices often employ a continuous graphene sheet or patches over the metasurface, which, as we also found, dampens the resonant behavior.

Interestingly, the voltage dependence of the device tuneability (Fig. 5c–f) has two distinct regions. In the low voltage window from 0 to 3 V, little change is observed. However, in the 3 to 6 V window, the changes are more profound and linear. The fitted resonance amplitude increases from around –18 to –25 dB and shifts from 0.192 to 0.187 THz. The Q-factor follows a similar trend, rising from 12 to 19, as reflected in the FWHM being reduced by 41%. A large amplitude tuning of the bilayer metasurface absorber is achieved with a low voltage range (3–6 V) and is reversible. This is a significant achievement as weaker tuning has been previously demonstrated using graphene, with higher bias voltages<sup>10,11,14,25,27,32,33</sup> or chemical doping<sup>32</sup>.

It is known that at THz frequencies, graphene's conductivity follows a Drude-like behavior, dominated by intraband transitions<sup>10</sup>. An applied voltage can be used to alter the Fermi level and, therefore, the intraband conductivity of the graphene. This cannot occur within the gold layer, suggesting that graphene is responsible for all tuning mechanisms. Altering the graphene conductivity in the bilayer results in two tuning effects. The first effect arises from the equivalent resistance ( $R_A$ ) of the RLC resonant circuit model. The change of the conductivity in the voltage-biased graphene/gold bilayer (upper electrode) varies the impedance matching of the resonant structure to the wave impedance of the THz radiation. This alters the resonant amplitude, as predicted by the RLC resonant circuit model. The second effect is an enhanced graphene intraband conductivity absorption of the THz wave and this effect is broadband. Changing graphene's intraband conductivity alters the absorption of the THz radiation. This occurs across the whole measured THz range (0.1–1 THz), including resonant and non-resonant regions. The observed device tuning of the resonant amplitude (16 dB) is a superposition of these two effects.

The experimental data agrees well with the simulation results shown in Fig. 3. The simulated peak amplitude changes from –17 to –22 dB corresponding to a graphene conductance varying from 40 to 100 mS. These are close to the experimentally observed values of –18 dB unbiased and –25 dB at 6 V bias resonant amplitudes. We approximate that the total experimental tuning range of the graphene conductivity in the bilayer is in the order of 60–75 mS for the 6 V applied voltage. This is significant as a similarly biased standalone graphene film (not in a bilayer) showed 5 mS tuning for 24 V applied (see Supplementary Fig. 1b). This suggests that the bilayer configuration enhances the achievable graphene conductivity tuning range. It should be noted that the comparison is made with the numerically fitted peaks (as in Fig. 5c–f), which accounts for the changing baseline from the broadband graphene absorption.

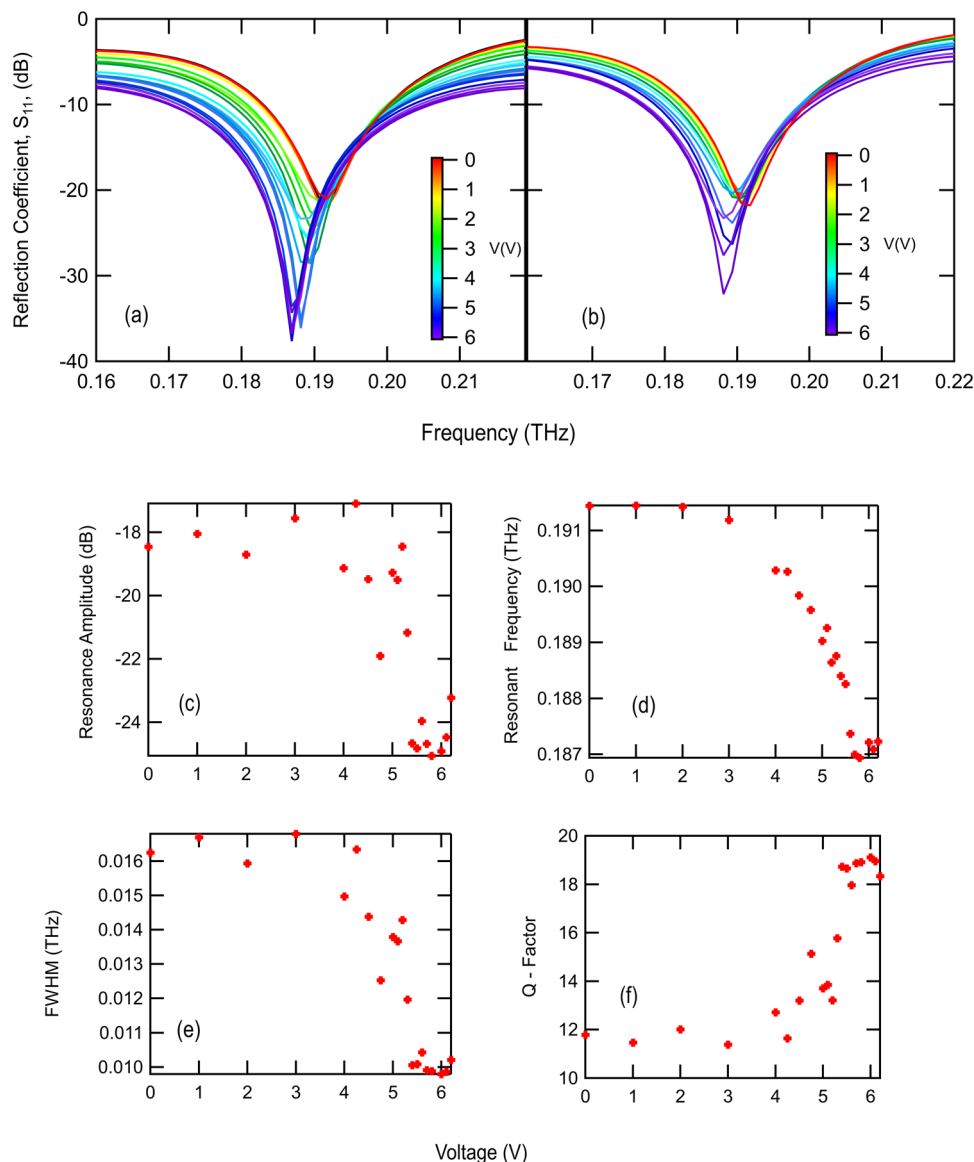


**Fig. 5** Experimental tuning performance of the graphene/gold bilayer metasurface device at 0.2 THz. **a, b**  $S_{11}$  parameter (power ratio) of the 0.2 THz resonance under varying bias voltage, showing clear frequency and amplitude tuning. In **(b)**, the voltage polarity is reversed with respect to **(a)**. **c-f** Voltage dependence of the **(c)** Resonance amplitude ( $\pm 0.3$  dB), **(d)** resonant frequency ( $\pm 2 \times 10^{-4}$  THz), **(e)** FWHM ( $\pm 3 \times 10^{-4}$  THz), and **(f)** Q-factor ( $\pm 0.5$ ) showing a flat response up to 3 V with observed linear behavior in the region above an applied voltage of 3 V. Parameters in **(c-f)** are obtained from peak fitting of the data in **(a)**.

It is noted that the device also demonstrated up to 5 GHz frequency tunability with a bias of 6 V, which suggests the bilayer approach can also be leveraged to produce frequency tunable devices. In the simulation, the RLC model only considered changes to the real part of the variable graphene conductivity. That is, the real resistive component ( $R_A$ ) is altered from the real part of the graphene conductivity (i.e., the real conductivity as shown in Supplementary Fig. 1a). A higher  $R_A$  from the tuned graphene in the bilayer produces a slightly higher resonant frequency in the simulation, as observed in Fig. 3. Experimental THz-TDS measurements of graphene's complex conductivity at a 24 V bias condition revealed that the imaginary part of the graphene conductivity also increases slightly with applied voltage (see Supplementary Fig. 1c). This increase, resulted from inductive and capacitive changes in the graphene, influences the impedance matching condition between the THz waves and absorber structure giving a decrease of the resonator frequency as

observed in the experimental data in Fig. 5. In this work, we mainly designed a frequency-selective amplitude-tunable metamaterial absorber to verify the superiority of the graphene/gold bilayer configuration, and the experimental data of the tuneability in amplitude agrees well with theoretical prediction. An improved RLC model that takes into consideration both the real and imaginary conductivity changes of the graphene film would better predict the resonator frequency shift. Purposely designed frequency-tuneable devices will need to account for the changes in the imaginary part of the graphene conductivity, which will be investigated in future research.

**Broadband response.** While the metadvice design and modeling focused on the 0.2 THz region, higher-order resonances and broadband characteristics were observed. Auxiliary modes were found at 0.36 THz, 0.40 THz, and 0.56 THz (Fig. 6a). These resonances also exhibited tuneability with applied voltage,

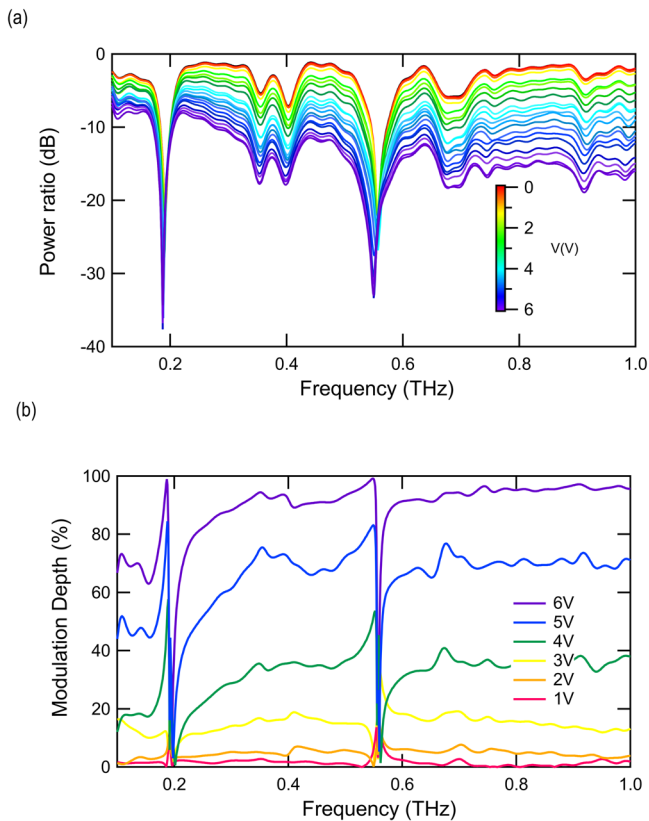


**Fig. 6 Broadband tuning performance of the graphene/gold bilayer metasurface device. a** Broadband frequency response of the absorber from 0 to 6 V. Frequency and amplitude tuning is observed for each resonance superimposed on a broadband modulation. **b** Broadband modulation depth of the graphene/gold bilayer absorber. Discontinuities are seen at resonant frequencies due to the relative frequency shift of these modes with respect to the applied field.

although less pronounced. The Q-factor of these higher modes was still above previously reported graphene THz metamaterial devices. From this response, we expect that the bilayer structure would be suitable for high Q-factor resonant devices up to at least 0.56 THz (the highest frequency resonance we measured and analyzed).

As with the 0.2 THz mode, there is a dual tuning effect across the higher-order modes from changes in the RLC impedance matching and intraband conductivity absorption. The broader spectrum shows that tuning by the RLC resonator effect is more dominant towards lower frequencies (stronger change in 0.2 THz than higher-order modes) and the contribution by intraband THz absorption of graphene becomes increasingly significant at higher THz frequency bands (larger changes of non-resonant regions in higher frequencies, as shown in Fig. 6). This is confirmed in the modulation depth of the non-resonating regions between 0.23–0.32 THz, 0.43–0.50 THz and 0.72–1 THz (Fig. 6b). The modulation depth is defined as  $MD = \frac{100 \times |\text{Ref}(0V) - \text{Ref}(6V)|}{\text{Ref}(0V)}$ , where  $\text{Ref}(V)$  is the THz reflectance at a voltage  $V$ . MD from 0.23–0.32 THz is 85%, 91% from 0.43–0.50 THz, and 95% above 0.72 THz. There is a clear frequency dependence on the modulation behavior of the bilayer, driven by the tuneable intraband conductivity, where modulation depth increases with photon energy. The strength of the tuneable broadband response up to 1 THz suggests the bilayer approach can be adapted for devices from 0.1–1 THz and potentially above 1 THz.

## Conclusion

In this work, we have presented a bilayer metamaterial structure where the whole device pattern has been superimposed into a 2D material, graphene, and gold. To the best of our knowledge, this is the first experimental demonstration of a THz communications device (0.1–1 THz) where the graphene is patterned into the entire device's metastructure. The bilayer structure circumvents the lack of tuneability in a gold-only metastructure and the poor performance of a graphene-only metastructure or graphene patches. As such, the experimentally developed graphene/gold bilayer THz frequency-selective absorber demonstrates tuning performance of over 16 dB at just 6 V bias voltage while maintaining a benchmark high Q-factor of 19 (compared to Q-factor  $<7$  for current graphene-based tuneable THz metasurfaces). The device also features broadband tuning exceeding 95% with the same low 6 V bias. The experimental results agree well with theoretical modeling results, which validates the theoretical prediction of the tunability for the bilayer metamaterial configuration. The graphene/gold bilayer concept and the fabrication methods can be adapted to numerous metamaterial THz devices theoretically modelled in the literature. The present work advances the new material and device technologies, which will impact emerging fields such as THz wireless communications, satellite target tracking, and sensing.

## Methods

**Graphene synthesis and characterization.** Graphene films were produced in-house using a Nickel catalyzed CVD process (99% purity, annealed). The graphene synthesis process is similar to that shown by ref. 24. In the present work, a modified atmospheric pressure, ambient air-based graphene synthesis process was used where an initial vacuum step was introduced and linoleic acid dissolved in ethanol (60% v/v) was substituted for soybean oil. Characterization of the materials (SEM and Raman mapping; see Supplementary Figs. 4–6) was carried out, confirming they were of good quality and continuous. This was performed at each step in the fabrication process: before transfer, after transfer, and post-fabrication.

Terahertz characterization of the graphene films was performed on a fiber-coupled time-domain spectroscopy (TDS) system in transmission geometry. Photoconductive antennae were utilized for both THz production and photodetection. Graphene films were transferred onto a PTFE substrate. The substrate was designed to be 3 mm thick to achieve an optimal trade-off between the measured signal and avoiding back reflections in the time-domain signal. Following the process outlined by ref. 34, the complex conductivity of the graphene film is extracted, and subsequently, the scattering rate, carrier mobility, and carrier density. From THz-TDS, the carrier mobility and carrier density were  $1393 \text{ cm}^2 \text{ V}^{-1} \text{ S}^{-1}$  and  $17 \times 10^{13} \text{ cm}^{-2}$ , respectively. These were obtained from the DC conductivity of 37 mS and a scattering time of 209 fs (scattering rate of 0.76 THz). These are reasonable values expected from CVD graphene, consistent with other reports in the literature<sup>35–39</sup>.

**Terahertz characterization.** Terahertz (THz) characterization of the device was performed on a fiber-coupled time-domain spectroscopy (TDS) system in reflection geometry as depicted in Fig. 7. Photoconductive antennae were utilized for both THz production and photodetection. To quantify the performance of the absorber, the reflected power of the electromagnetic wave,  $\bar{E}^{\text{Ref}}(\omega)$ , of the metasurface device,  $\bar{E}_{\text{MS}}^{\text{Ref}}(\omega)$ , is ratioed to a reference measurement ( $\bar{E}_{\text{Ref}}^{\text{Ref}}(\omega)$ ), made with a gold-backed Rogers 5880LZ substrate with no bilayer metasurface. We consider the absorber to be a single-port device, with a corresponding  $S_{11}$  parameter, given through the relation  $S_{11} = 10 \log(R)$ . Here  $R$  is the ratio (reflectance) of the sample and reference power spectrum,  $R = \frac{\bar{E}_{\text{MS}}^{\text{Ref}}(\omega)^2}{\bar{E}_{\text{Ref}}^{\text{Ref}}(\omega)^2}$ . For tuneability, the process is repeated incrementally from 0 to 6 V, applying the bias voltage to the contacts fabricated into the device. The raw spectral data can be found in Supplementary Fig. 7.

**Simulation.** Three-dimensional full-wave modeling and simulations were performed using CST Microwave Studio, which is based on the finite-difference time-domain method. Within the model, the top layer is a graphene/gold bilayer patterned with Jerusalem-cross slots in a periodical arrangement, while the bottom layer is a perfect gold layer forming an RF ground. The graphene part was treated as a thin film with a thickness of 50 nm (from surface profiler measurement) and a specific surface conductivity as quantified from the complex conductivity obtained by THz time-domain spectroscopy. The real and imaginary parts of the graphene surface conductivity in the region of interest (0.1–0.3 THz) were observed to be 37 and 10 mS, respectively. The gold layers were modeled as zero-thickness sheets

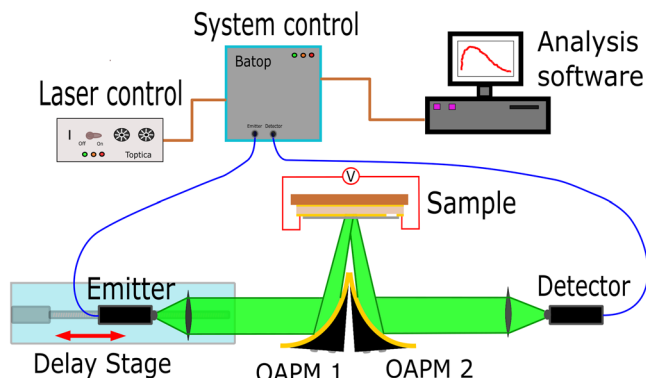


**Fig. 7 Experimental setup for device measurement.** Terahertz time-domain spectroscopy in reflection geometry. The THz wave is emitted and detected by photoconductive antennae (PCAs), with the THz beam focussed (~5 mm spot size) and re-collected from the sample via two off-axis paraboloid mirrors (OAPM 1 and 2). In this setup, the graphene/gold bilayer metasurface frequency-selective absorber acts as a single-port electrical device.

with an electrical conductivity of  $4.5 \times 10^7 \text{ Sm}^{-1}$ . The Rogers5880 substrate with a thickness of 0.254 mm is modeled with a relative permittivity and loss tangent of 2.3 and 0.02 at the THz band, respectively.

### Data availability

The datasets generated and/or analyzed during the current study are available from the corresponding authors on reasonable request, or can be accessed via <https://doi.org/10.25919/1kqc-ht18>.

Received: 30 June 2022; Accepted: 1 August 2022;

Published online: 20 August 2022

### References

- Nagatsuma, T., Ducournau, G. & Renaud, C. C. Advances in terahertz communications accelerated by photonics. *Nat. Photonics*. **10**, 371–379 (2016).
- Yang, Y. et al. Terahertz topological photonics for on-chip communication. *Nat. Photonics*. **14**, 446–451 (2020).
- Aghasi, H. et al. Terahertz electronics: application of wave propagation and nonlinear processes. *Appl. Phys. Rev.* **7**, 021302 (2020).
- Ebrahimi, A. et al. High-Q terahertz absorber with stable angular response. *IEEE Trans. Terahertz Sci. Technol.* **10**, 204–211 (2020).
- Sengupta, K., Nagatsuma, T. & Mittleman, D. M. Terahertz integrated electronic and hybrid electronic-photonic systems. *Nat. Electron.* **1**, 622–635 (2018).
- Cheben, P., Halir, R., Schmid, J. H., Atwater, H. A. & Smith, D. R. Subwavelength integrated photonics. *Nature* **560**, 565–572 (2018).
- He, J., Dong, T., Chi, B. & Zhang, Y. Metasurfaces for terahertz wavefront modulation: a review. *J. Infrared Millim. Terahertz Waves* **41**, 607–631 (2020).
- Bao, L. & Cui, T. J. Tunable, reconfigurable, and programmable metamaterials. *Microw. Opt. Technol. Lett.* **62**, 9–32 (2020).
- He, X. Tunable terahertz graphene metamaterials. *Carbon* **82**, 229–237 (2015).
- Sensale-Rodriguez, B. et al. Broadband graphene terahertz modulators enabled by intraband transitions. *Nat. Commun.* **3**, 780 (2012).
- Sensale-Rodriguez, B. et al. Extraordinary control of terahertz beam reflectance in graphene electro-absorption modulators. *Nano Lett.* **12**, 4518–4522 (2012).
- Chen, Z. et al. Graphene controlled Brewster angle device for ultra broadband terahertz modulation. *Nat. Commun.* **9**, 4909 (2018).
- Di Gaspare, A. et al. Tunable, grating-gated, graphene-on-polyimide terahertz modulators. *Adv. Funct. Mater.* **31**, 2008039 (2021).
- Gómez-Díaz, J. S. et al. Self-biased reconfigurable graphene stacks for terahertz plasmonics. *Nat. Commun.* **6**, 6334 (2015).
- Qian, Z., Yang, D. & Wang, W. Terahertz modulation based on surface plasmon resonance by self-gated graphene. *Opt. Commun.* **414**, 52–58 (2018).
- He, X., Liu, F., Lin, F. & Shi, W. Tunable high Q-factor terahertz complementary graphene metamaterial. *Nanotechnology* **29**, 485205 (2018).
- Cai, Y. & Xu, K. D. Tunable broadband terahertz absorber based on multilayer graphene-sandwiched plasmonic structure. *Opt. Express* **26**, 31693–31705 (2018).
- Wei, Z. et al. Active plasmonic band-stop filters based on graphene metamaterial at THz wavelengths. *Opt. Express* **24**, 14344–14351 (2016).
- Chen, D. et al. The novel graphene metasurfaces based on split-ring resonators for tunable polarization switching and beam steering at terahertz frequencies. *Carbon* **154**, 350–356 (2019).
- Tang, P. R. et al. Ultrasensitive specific terahertz sensor based on tunable plasmon induced transparency of a graphene micro-ribbon array structure. *Opt. Express* **26**, 30655–30666 (2018).
- Melnikov, L. & Nefedov, I. Plasmonic terahertz amplification in graphene-based asymmetric hyperbolic metamaterial. *Photonics* **2**, 594–603 (2015).
- Radwan, A., Verri, V., D'Amico, M. & Gentili, G. G. Beam reconfigurable antenna for the THz band based on a graphene high impedance surface. *Phys. E*. **85**, 316–323 (2017).
- Levchenko, I. et al. Scalable graphene production: perspectives and challenges of plasma applications. *Nanoscale* **8**, 10511–10527 (2016).
- Seo, D. H. et al. Single-step ambient-air synthesis of graphene from renewable precursors as electrochemical gas sensor. *Nat. Commun.* **8**, 14217 (2017).
- Kindness, S. J. et al. Active control of electromagnetically induced transparency in a terahertz metamaterial array with graphene for continuous resonance frequency tuning. *Adv. Opt. Mater.* **6**, 1800570 (2018).
- Valmorra, F. et al. Low-bias active control of terahertz waves by coupling large-area CVD graphene to a terahertz metamaterial. *Nano Lett.* **13**, 3193–3198 (2013).
- Gao, W. et al. High-contrast terahertz wave modulation by gated graphene enhanced by extraordinary transmission through ring apertures. *Nano Lett.* **14**, 1242–1248 (2014).
- Degli-Innocenti, R. et al. Low-bias terahertz amplitude modulator based on split-ring resonators and graphene. *ACS Nano* **8**, 2548–2554 (2014).
- Gorecki, J. et al. Optically reconfigurable graphene/metal metasurface on Fe:LiNbO<sub>3</sub> for adaptive THz optics. *ACS Appl. Nano Mater.* **3**, 9494–9501 (2020).
- Liu, W. et al. Graphene-enabled electrically controlled terahertz meta-lens. *Photonics Res.* **6**, 703–708 (2018).
- Miao, Z. et al. Widely tunable terahertz phase modulation with gate-controlled graphene metasurfaces. *Phys. Rev. X* **5**, 041027 (2015).
- Arezoomandan, S. et al. Graphene–dielectric integrated terahertz metasurfaces. *Semicond. Sci. Technol.* **33**, 104007 (2018).
- Lee, S. H. et al. Switching terahertz waves with gate-controlled active graphene metamaterials. *Nat. Mater.* **11**, 936 (2012).
- Bøggild, P. et al. Mapping the electrical properties of large-area graphene. *2D Mater.* **4**, 042003 (2017).
- Arts, K. et al. Broadband optical response of graphene measured by terahertz time-domain spectroscopy and FTIR spectroscopy. *J. Appl. Phys.* **124**, 073105 (2018).
- Dadrasnia, E. & Lamela, H. Terahertz conductivity characterization of nanostructured graphene-like films for optoelectronic applications. *J. Nanophotonics* **9**, 093598 (2015).
- Dadrasnia, E. et al. Sub-THz characterisation of monolayer graphene. *J. Spectrosc.* **2014**, 1–6 (2014).
- Abouelsayed, A. et al. Preparation, characterization, Raman, and terahertz spectroscopy study on carbon nanotubes, graphene nano-sheets, and onion like carbon materials. *Mater. Chem. Phys.* **189**, 127–135 (2017).
- Liang, M. et al. Terahertz characterization of single-walled carbon nanotube and graphene on-substrate thin films. *IEEE Trans. Microwave Theory Tech.* **59**, 2719–2725 (2011).

### Acknowledgements

A.D.S. acknowledges the CSIRO CERC Postdoctoral Fellowship Program. D.H.S. acknowledges the support from UTS Chancellor Fellowship. The authors acknowledge cleanroom fabrication assistance from Ms. J. Lazar and THz setup assistance from Dr. K. Radhanpura and Dr. D. Farrant. The authors acknowledge the facilities as well as the scientific and technical assistance of the Research and Prototype Foundry Core Research Facility at the University of Sydney, part of the NSW node of the NCRIS-enabled Australian National Fabrication Facility.

### Author contributions

A.D.S. fabricated the bilayer metasurface absorber device. A.D.S. carried out Terahertz device characterization and analysis. A.D.S., J.D., and T.v.d.L. developed the fabrication procedure, including patterning of the graphene/gold bilayer metastructure. J.D. conceived the project idea. X.G. designed the device and performed the modeling with inputs from A.D.S., J.D., and T.Z. T.v.d.L., D.H.S., J.S.C., and A.T.M. performed and optimized the graphene synthesis, transfer to the substrate, and graphene characterization/analysis. S.K.H.L. assisted in fabrication. A.D.S. wrote the manuscript supported by X.G., J.D., Z.H., and T.v.d.L.

### Competing interests

A.D.S, J.D., and T.v.d.L declare the following competing financial interest: The frequency-selective absorber device presented is subject to an Australian Provisional Patent Application (2021901438) titled “Device for interacting with electromagnetic radiation.”

### Additional information

**Supplementary information** The online version contains supplementary material available at <https://doi.org/10.1038/s43246-022-00279-7>.

**Correspondence** and requests for materials should be addressed to Andrew D. Squires or Timvander Laan.

**Peer review information** *Communications Materials* thanks the anonymous reviewers for their contribution to the peer review of this work. Primary Handling Editor: John Plummer. Peer reviewer reports are available.

**Reprints and permission information** is available at <http://www.nature.com/reprints>

**Publisher’s note** Springer Nature remains neutral with regard to jurisdictional claims in published maps and institutional affiliations.



**Open Access** This article is licensed under a Creative Commons Attribution 4.0 International License, which permits use, sharing, adaptation, distribution and reproduction in any medium or format, as long as you give appropriate credit to the original author(s) and the source, provide a link to the Creative Commons license, and indicate if changes were made. The images or other third party material in this article are included in the article’s Creative Commons license, unless indicated otherwise in a credit line to the material. If material is not included in the article’s Creative Commons license and your intended use is not permitted by statutory regulation or exceeds the permitted use, you will need to obtain permission directly from the copyright holder. To view a copy of this license, visit <http://creativecommons.org/licenses/by/4.0/>.

© Crown 2022